Research Article | Vol. 34, No. 6 / 23 Mar 2026 / Optics Express 10103
Optics EXPRESS

Coherent modal engineering: a perspective on fiber splice optimization

VINCENZO SCARNERA,[1,3] CHRISTOPHE A. CODEMARD,[2,3] AND MICHALIS N. ZERVAS[1,2,*]

[1]Optoelectronics Research Center, University of Southampton, Southampton, UK
[2]Advanced Laser Lab, ORC/Trumpf Lasers UK, University of Southampton, Southampton, UK
[3]TRUMPF Lasers UK, Wellington Park, Toolbar Way, Hedge End, Southampton, UK
*mnz@soton.ac.uk

Abstract: In this work, we introduce a coherent modal engineering approach to optimize single-mode to multimode doped fiber splices. By systematically varying the arc duration and analyzing higher-order mode excitation using the S^2 technique, we reveal that the optimal splicing condition does not correspond to matched mode field diameters at the splice interface, as traditionally assumed. Instead, measurements of the thermally diffused refractive index profiles show that the multimode fiber undergoes a longitudinally non-adiabatic index transition, leading to coupling from the fundamental mode (LP_{01}) into higher-order modes (particularly LP_{02}). We demonstrate that the optimal arc duration creates a deliberate mode-field-diameter mismatch that excites LP_{02} with a tailored amplitude and phase—precisely configured to destructively interfere with the higher-order-mode content generated in the non-adiabatic region. This controlled interference mechanism forms the basis of a splice optimization paradigm that prioritizes modal coherence and beating over geometric matching.

1. Introduction

Efficient and reliable splicing between dissimilar optical fibers is a fundamental requirement for constructing high-performance fiber amplifiers and laser systems. In particular, low-loss fusion splicing is critical for ensuring optimal power transfer, long-term operational stability, and beam quality preservation under high optical powers. Traditional splice optimization involves empirical tuning of arc parameters - such as current, duration, and alignment – to diffuse locally the core and minimize transmission loss, primarily through matching mode field diameters (MFDs) of the mating fibers on either side of the splice interface thus yielding optimal performance [1–7]. It is shown that the arc temperature and duration, in particular, affect considerably the transmission loss and splice quality between single-mode fibers (SMFs) as they control the viscous flow of SiO_2 in forming the joint between the mating fibers and the diffusion of the glass-forming co-dopants altering the refractive index profile (RIP) [8]. It has also been shown that the overall splice loss of two dissimilar SMFs can be influenced by interference of the fundamental mode with radiation modes generated by the MFD mismatch [9], in a manner similar to observed SMF bending loss non-monotonic (oscillating) variations with bending radius [10].

However, the splicing process becomes even more complex in doped fiber systems, where thermally driven dopant diffusion during splicing modifies the refractive index profile (RIP) near the joint, altering local mode properties and propagation behavior [5–7]. The challenge is further exacerbated when SMFs are spliced to multi-mode doped fibers (MMFs), an architecture prevalent in high-power fiber lasers and amplifiers [11]. Most active fibers, used in high power lasers and amplifiers, have large core areas (to reduce optical nonlinearities) and high core NA (due to high dopant concentrations, needed to reduce length), which inevitably result in

#589926 https://doi.org/10.1364/OE.589926
Journal © 2026 Received 13 Jan 2026; revised 19 Feb 2026; accepted 27 Feb 2026; published 12 Mar 2026

Optics EXPRESS

multimode guidance. In addition, passive SMF or quasi-SMF pigtails are used to ensure high beam quality outputs. In these systems, the excitation of unwanted higher-order modes (HOMs) is not always apparent in transmission loss measurements, since they can be captured and be guided by the core, thus contributing negligibly to the overall transmission loss. However, their excitation can profoundly impact system performance by triggering modal gain competition and transverse modal instabilities (TMI) [11–13]. This renders conventional transmission-loss-based optimization strategies inadequate in this case.

In this study, we report a new strategy for optimizing SMF-to-MM doped fiber splicing by explicitly addressing HOM excitation contributions. Using the S^2 imaging technique [14], we quantify the modal content as a function of arc duration and analyze the corresponding thermally induced RIP changes. Surprisingly, we find that the splice arc condition that minimizes HOM excitation does not correspond to a matched MFD configuration. Instead, we demonstrate that the optimal splice occurs when a deliberate MFD mismatch excites the LP_{02} mode with an amplitude and phase that destructively interferes with the HOM power generated in the longitudinally non-adiabatic RIP transition of the splice. This coherent modal engineering approach reveals a new principle for splice optimization that transcends traditional MFD matching and enables suppression of unwanted modes through precise thermal tailoring of the splice region. Our findings establish a new paradigm for designing low-HOM splices in high-power fiber systems, with direct implications for improving efficiency, repeatability, beam quality, power scalability, and modal control in next-generation fiber lasers.

In Section 2, we present the experimental splice optimization set-up and results. In Section 3, we discuss the detailed splice characterization and in-depth analysis of coherent modal effects and their impact on the modal output power optimization, by considering the effective mode areas and effective mode index differences along the splice length. Section 4 includes a summary and discussion of the main results. Finally in Supplement 1, we summarize the transfer matrix method, used for calculating the modal evolutions along the splice length, while in Appendix A we provide analysis of general two-port optical devices, using the scattering matrix approach, and use it to analytically optimize SMF-to-MMF splices.

2. Experimental splice optimization

Anticipating that HOM excitation will be critical to the optimization of SMF-to-MMF splices, we incorporated the fusion splicer into an S^2 measurement setup [14], as shown in Fig. 1(a). The output of a tunable laser source (TLS) (Newport TLB-6722) with less than 200 kHz linewidth, 1045nm-1085 nm scanning range and 25 mW maximum output power was delivered through a HI1060 10/125 µm to the SMF of interest to be spliced to an Yb^{3+}-doped MMF. The SMF and the doped MMF were part of the high-power fiber laser or amplifier. Both SMF and Yb^{3+}-doped MMF had matching cladding diameters of 200 µm. and centered through cladding alignment. Generally, at the SMF-to-MMF splice more than one mode will be excited and couple into the MMF. The multimode output is then imaged onto a CCD camera (Thorlabs BSC106) by a couple of plane-convex lenses having a combined magnification of 200, while a neutral density (ND) filter is used to attenuate the laser light. Figure 1(b) illustrates a typical multipath interference (MPI) measurement, showing the splice-induced relative modal excitation levels of the modes excited at the splice point.

In all cases, the MPI maps show all the supported HOMs, albeit at substantially different excitation levels (modes LP_{21}, LP_{31} and LP_{03} are consistently ~2 orders of magnitude lower than LP_{02} and LP_{11}). The results in Fig. 1(b) were obtained with an intentionally misaligned splice, showing excitation of LP_{02} and LP_{11} modes at about the same level. However, properly cladding-aligned splices show LP_{11} mode excitation substantially lower than the corresponding LP_{02} mode level (see Figs. 2(b) & (c) below).

Optics EXPRESS

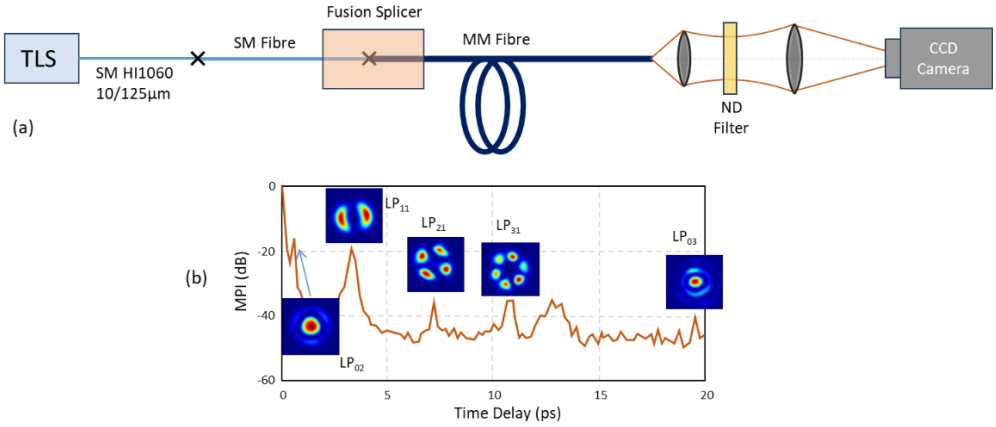

Fig. 1. (a) Experimental set-up incorporating the splicer into an S^2 measurement set up; (b) typical MPI measurement.

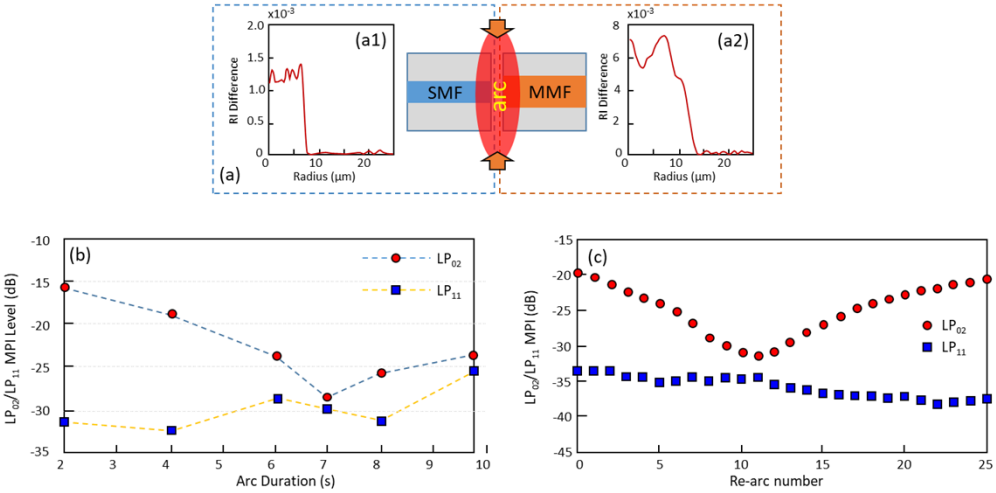

Fig. 2. (a) SMF-to-MMF splice schematic showing the RIPs for the SMF (a1-left) and MMF (a2-right); LP_{02} and LP_{11} MPI level as a function of (b) single arc duration (Case 1) and (c) number of short arcs (Case 2), at fixed current.

A systematic study of splice optimization was carried out, and the results are shown in Fig. 2. RIPs of the passive germano-silicate SMF and ytterbium-doped phospho-silicate MMF under study, measured with a commercial profilometer (IFA-100), are shown in Fig. 2(a1) and 2(a2), respectively. At the operating wavelength of 1070 nm, the SMF is single-moded, while the MMF supports 6 linearly-polarized (LP) modes. Two different splice optimization strategies were investigated using the same SMF/MMF pair. An in-house modified cleaver was used to achieve cleave angles below 0.1° in every optimization experiment, as measured by the fusion splicer prior to splicing. In both cases the arc current was kept constant. In the first case a single arc with varying duration for the different splices was employed, while in the second one multiple arcs with short, fixed duration on a single splice were applied. It should also be remarked that usually the temperature radial profile is peaked and bell-shaped but flattened in the very center because of high thermal conductivity in fully ionized plasma. It typically follows a quasi-parabolic radial

Optics EXPRESS

profile and a steep gradient over just a few millimeters [15]. Details of the temperature radial profile can be important as they can define the dopant diffusion distribution along the splice length. In all cases, the modal excitations, determined by the level of the MPI peaks of the MM fiber, were measured by the S^2 technique [14].

2.1. Case 1: single arc with varying duration – different splices

Six different splices have been produced between lengths of the same SM/MM fibers using different arc durations and keeping the same current, ensuring that the degree of diffusion is primarily determined by the arc duration. In Fig. 2(b), the MPI level of the dominant LP_{02} and weaker LP_{11} mode is plotted as a function of the arc duration, showing that the 7s arc duration splice has minimum LP_{02} content. Increasing the arc duration above 7s results in a higher LP_{02} mode excitation and splice performance deterioration. The different splices require re-stripping and re-cleaving of the fibers, which gives slightly different cleave angles, as well as core-to-core concentricity, and predominantly accounts for the spread of the LP_{11} MPI level.

2.2. Case 2: multiple arcs with fixed short duration – same splice

In a different experiment, we used an initial arc of 4 seconds, joining the fibers and then a series of shorter re-arcs lasting one second each. Between each re-arc the modal excitation was measured. Figure 2(c) shows a typical MPI variation for the dominant LP_{02} and LP_{11} modes as a function of the number of short re-arcs. Point 0 is the one obtained after the initial 4s arc. It is shown that the LP_{02} mode excitation level reduces to a minimum at an optimum number of arcs (~11 arcs in this case) and increases again when this number is exceeded. The LP_{11} mode excitation level, on the other hand, remains largely unaffected. The observed slight improvement is due to core-to-core concentricity improvements through repeated arching.

Comparison of the results in Figs. 2(b) and (c) shows that multiple short re-arcs (Case 2) result in a more controlled splicing process with lower LP_{02} and LP_{11} MPI levels and superior splice quality. In both cases, the optimum arcing conditions correspond to the lowest LP_{02} mode excitation, as this ensures lowest modal gain competition and highest overall efficiency and stability.

3. Splice characterization and analysis

In Case 1, all splices were fully characterized by measuring RIPs every 20 μm along their length via an IFA-100 instrument. Representative results for the arc duration of 7s are shown in Fig. 3(a). Severe RIP variation, due to dopant diffusion, is observed in the MM fiber close to the splice point in the $0 < z < 700$μm region, marked as "diffused region". Beyond 700μm the MM fiber remains mostly undiffused (marked as "mildly-diffused region").

Figure 3(b) shows RIPs at specific points along the splice. It is observed that the degree of diffusion of the MM fiber increases as the splice point ($z = 0$) is approached (c.f. Figure 3(b6) -(b3)). The RIP of the SM fiber, on the other hand, is only affected at points adjacent to the splice point ($z = 0$) (c.f. Figure 3(b2) - (b1)). The observed core burnout is believed to be predominantly due to longitudinal SiO_2 flow and diffusion into the MM fiber core [1,8]. RIPs measured along the splice length were used to calculate local fiber modes [16] and the corresponding mode profiles for the LP_{01} and LP_{02} modes are shown in Fig. 3(c1-c6). As expected, the field distributions are affected significantly by the diffusion process. Knowledge of the local modes allows computing field evolutions, effective mode areas and power exchange between propagating modes, by means of a transfer-matrix method (TMM) [16,17], summarized in Supplement 1.

Figures 4(a) and (b) show the calculated relative power at the splice output for the LP_{02} and LP_{01} modes, respectively, as a function of the arc duration, each time using the corresponding measured RIP distribution. In Fig. 4(a), the experimentally obtained MPI peak values are replotted, showing a very good agreement between the overall trends and the experimental

Optics EXPRESS

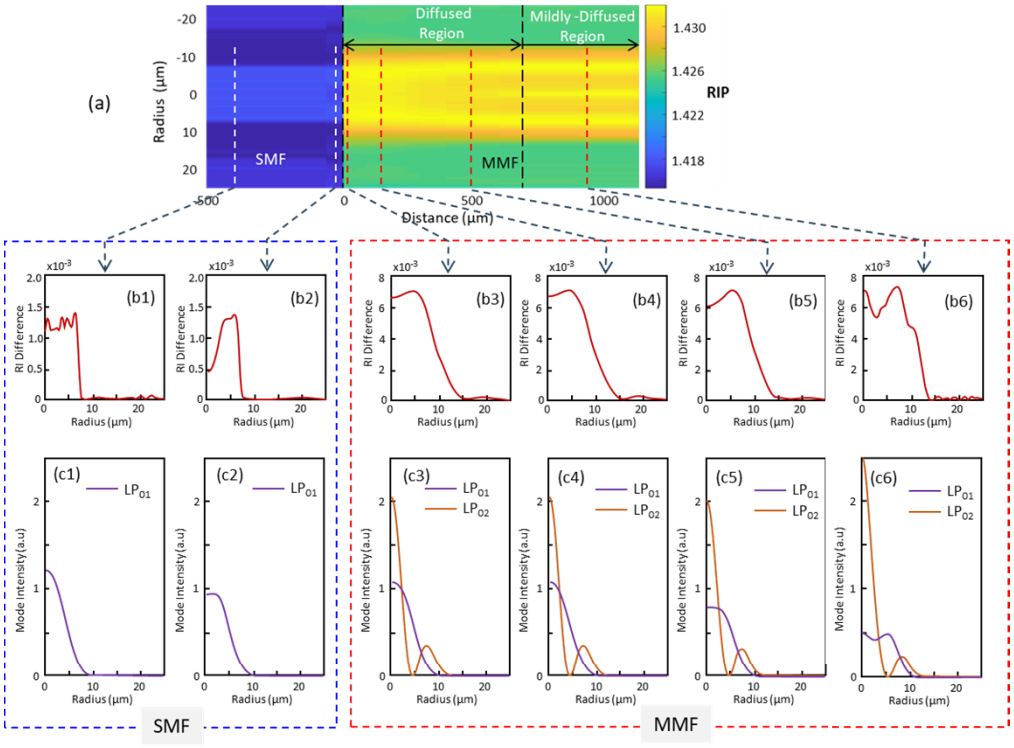

Fig. 3. (a) Measured RIP around the splice point (z = 0); (b) RIP at specific positions; (c) calculated intensity profiles at the corresponding splice positions. Arc duration 7s.

/calculated optimum arc duration (7 s). The observed offset is due to the rather coarse splice segmentation used in the TMM calculations. Figure 4(b) does not show experimental LP_{01} values, since the S^2 technique only provides the LP_{02} power relative to the LP_{01} one, without measuring explicitly the latter.

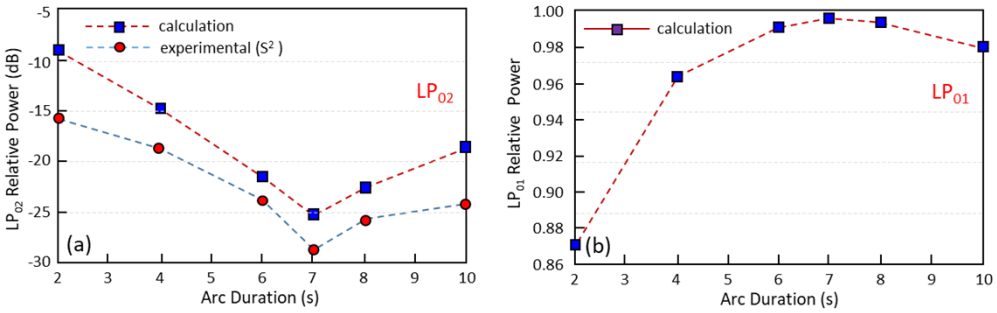

Fig. 4. (a) Calculated and experimental relative powers at the splice output for LP_{02} mode and (b) calculated relative power at the splice output for LP_{01} mode as a function of the arc duration.

Optics EXPRESS

3.1. Effective mode areas and effective mode index differences

To better understand the conditions under which the optimum splice performance occurs, the modal intensities $I_{mn}(r, \varphi, z)$ of the LP_{mn} mode are used to calculate the corresponding effective mode areas (EMA), defined as $A_{mn}^{eff}(z) = \left[\int_0^{2\pi}\int_0^{\infty} I_{mn}(r,\varphi,z) r dr d\varphi\right]^2 / \int_0^{2\pi}\int_0^{\infty} |I_{mn}(r,\varphi,z)|^2 r dr d\varphi$.

Figure 5(a) plots the LP_{01} EMA variation and Fig. 5(b) plots the corresponding LP_{01}/LP_{02} effective mode index difference $\Delta n_{eff} = n_{eff}^{01} - n_{eff}^{02}$, around the splice point (z = 0). In Fig. 5(a), it is first observed that the LP_{01} EMA varies significantly along the diffused region of the doped MM fiber (z > 0), as the arc duration increases. The LP_{01} EMA in the SMF side of the splice (z < 0), on the other hand, shows minimal variation, despite the observed core burnout, and does not impact significantly the overall analysis. It is known that, under similar temperature conditions, the diffusion coefficient of GeO_2 (z < 0) is about an order magnitude smaller than the one of P_2O_5 (z > 0) [18,19]. We also observe that the initial large EMA mismatch ($\approx 140\mu m^2/250\mu m^2$) between the SMF/MMF at the splice point z = 0 decreases monotonically with the arc duration. Assuming that the splice quality depends primarily on the EMA mismatch [3–6], we would have expected a similar monotonic decrease in LP_{02} mode excitation. However, it is important to notice that at the optimum arc duration of 7s (LP_{02} MPI ≈ -28 dB) there is still a substantial LP_{01} EMA mismatch ($\approx 150\mu m^2/180\mu m^2$) between the SMF/MMF sides of the splice point. On the other hand, at the arc duration of 10s, which results in an almost perfect EMA matching ($\approx 160\ \mu m^2/155\mu m^2$), the splice performance is deteriorated (LP_{02} MPI ≈ -24 dB). These rather counter-intuitive results are in sharp contrast with the current understanding of splice optimization [3–6] and as such they require further consideration.

3.2. Coherent modal effects

Using experimental RIPs and calculated modal fields, we next investigate the evolution and relative powers of the LP_{01} mode along the entire splice length, as well as the LP_{02} mode initially excited at z = 0 due the LP_{01} mode EMA mismatches. Figures 6(a) and (b) plot the relative LP_{02} and LP_{01} powers, respectively, as a function of distance along the splice length. It is observed that the initially excited LP_{02} relative power decreases monotonically with the arc duration, as a direct result of the LP_{01} SMF/MMF EMA mismatch decrease at z = 0, as already seen in Fig. 5(a). It is also observed that the LP_{01} and LP_{02} power variations are negligible in regions I and III. This is due to the almost adiabatic propagation, as evidenced by the very small (region I) and gradual (region III) variations of the EMA and Δn_{eff} in these areas, shown in Figs. 6(a) and (b). The most significant power exchange between the LP_{01} and LP_{02} modes, on the other hand, takes place in region II, as a result of the non-adiabatic transition resulting from the much larger and steeper changes in the EMA and Δn_{eff}. It is also noticed that for arc durations of 2s to 7s, for which the splice performance improves, the LP_{02} power at the output (region III) is smaller than the initially excited one (region I). As shown in Fig. 6(b), this is due to gradual non-monotonic power transfer to LP_{01} mode in region II. For arc durations of 8s and 10s, on the other hand, the LP_{02} power at the output (region III) is larger than the initially excited one (region I). In this case, the improved EMA matching at z = 0 (see Fig. 5(a)) results in almost complete LP_{01} mode excitation in region I, which is then transferred gradually into LP_{02} over the strongly varying non-adiabatic region II (see Fig. 6).

To further appreciate the importance of the initial excitation of LP_{02} at z = 0 in the SMF/MMF splice optimization process, Fig. 7(a) and (b) plots the evolution of LP_{02} and LP_{01} relative powers as a function of the distance from the splice point without any initial LP_{02} excitation, i.e. LP_{01} only excitation. In this case, for arc duration of 2s there is no power exchange taking place, due to very small and gradual (and therefore adiabatic) transition (see Fig. 5(a)). For similar reasons, there have been no power exchanges in regions I and III for arc durations of 4s to 7s. For arc durations of 8s and 10s, there have been small power exchanges in region III, due to steeper variations in EMA (see Fig. 5(a)). For all arc durations, it is obvious that substantial

Optics EXPRESS

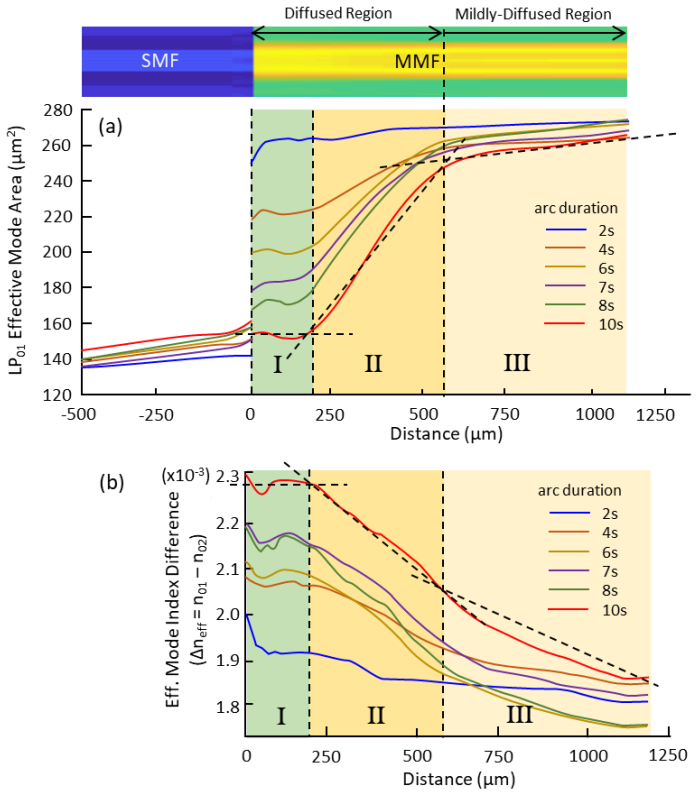

Fig. 5. (a) LP_{01} effective area variation around the splice point (z = 0); (b) effective mode index difference along the MM fiber length. I, II and III mark the predominantly uniform, non-adiabatic and quasi-adiabatic, respectively, splice transition regions.

LP_{01}/LP_{02} power exchange takes place only in region II, where the splice RIP and the EMA changes non-adiabatically. Increasing the arc duration results in steeper RIP and EMA variations and, therefore, increasingly larger power transfer.

From the results in Figs. 6 and 7, it is apparent that, under all circumstances, region I contributes only to the initial LP_{02} mode excitation, with magnitude depending on the EMA mismatch. It has also negligible effect on further LP_{01}/ LP_{02} power exchange, contributing only to a relative phase shift between the modes. This is due to the saturated and quasi-uniform RIP diffusion over this region (see Fig. 3(a)) and the corresponding almost constant EMA and Δn_{eff} over this region (see Fig. 5). It is also evident that substantial power exchanges take place only in the non-adiabatic region II. From this analysis, it has become obvious that in order to fully understand the optimization process in SM-to-MM fiber splices, the initial excitation of modes, due to LP_{01} EMA mismatches, the relative phasing of the modes, as well as the internal non-adiabatic power transfer between modes should be taken into account and properly engineered. It should be also mentioned at this point that the response of the splice in region II is akin to the performance of tapered coaxial optical fiber couplers [20,21].

3.3. *Modal output power optimization*

To further explore the importance of the initially excited LP_{02} mode in the performance of the SMF/MMF splice, in Fig. 8 we plot the variation of the LP_{02} and LP_{01} modes at the splice output as a function of the amplitude (p) and relative phase ($\Delta\theta$) of the initially excited LP_{02} mode

Optics EXPRESS

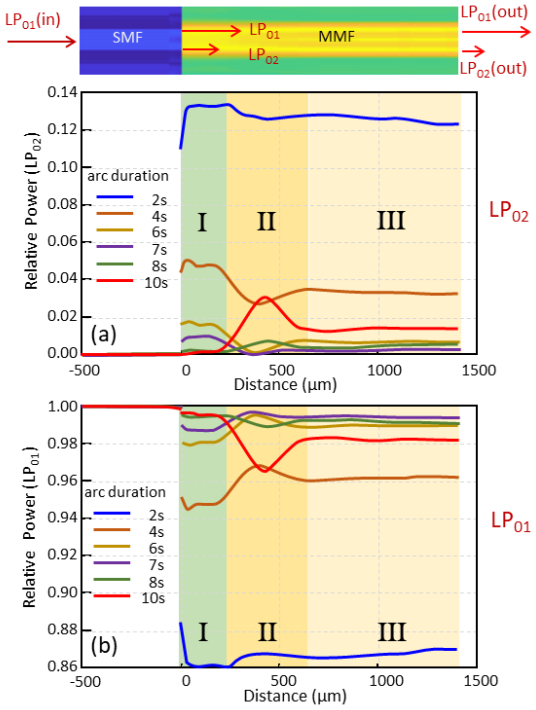

Fig. 6. Evolution of (a) LP_{02} and (b) LP_{01} relative powers, as a function of distance along the splice length. SMF/MMF LP_{01} modes are mismatched and both LP_{01} & LP_{02} are excited at SMF/MMF interface (z = 0).

at z = 0, for the measured splice RIP corresponding to arc duration of 7s, using the numerical TMM presented in Supplement 1. It is shown that the right combination of initially excited LP_{02} amplitude and relative phase ($p = 0.049$ (power about -26 dB) & $\Delta\theta = -25.5°$) at the input of the splice results in minimization of LP_{02} and maximization of LP_{01}, at the splice output. Under these optimum excitation conditions, the LP_{02} output power is about -71 dB, much lower than the experimentally obtained value of about -29 dB. It should be stressed that in the actual splice, the initial LP_{02} amplitude (p) is primarily determined by the EMA mismatch at z = 0, while the relative phase mismatch ($\Delta\theta$) is primarily determined by the propagation over the "saturated" almost flat region I, while the arc duration affects both the initial excitation and the relative phase. Even in the optimum case of 7s arc duration, the absolute LP_{02} minimum is missed. However, by increasing the arc duration (Case 1) or by appropriate post processing through multiple short re-arcing (Case 2) can trim the LP_{02} excitation parameters (p & $\Delta\theta$) and improve considerably the splice quality. In Fig. 8(a), the red superimposed line shows schematically a possible optimization path followed by progressively increasing the arc duration (Case 1) or number of short re-arcs (Case 2).

Similar optimization maps can be derived with all the splice RIPs obtained with the other arc durations, indicating that there is always an optimum LP_{02} initial excitation amplitude (p) and relative phase ($\Delta\theta$) that results in splice optimum performance, i.e. infinitesimally small LP_{02} and maximum LP_{01} powers. In Appendix A, it is shown that the optimum LP_{02} initial excitation amplitude (p) and relative phase ($\Delta\theta$) can be derived analytically by considering the SMF-to-MMF splice as a two-port reciprocal coupled system. In the lossless case, it is shown that the optimum initial excitation input LP_{01} and LP_{02} amplitudes are complex conjugate of the LP_{01} and LP_{02} output amplitudes when only LP_{01} mode is initially excited at the input.

Optics EXPRESS

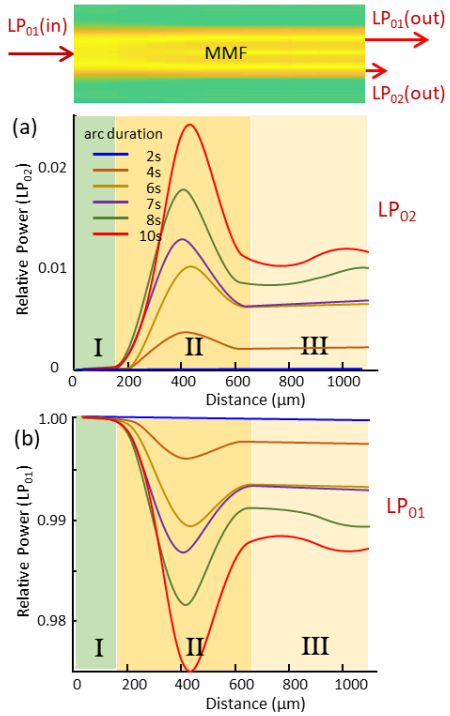

Fig. 7. Evolution of (a) LP_{02} and (b) LP_{01} relative modal powers as a function of the distance from the splice point without any initial LP_{02} excitation, i.e., LP_{01}-only excitation at SMF/MMF interface (z = 0).

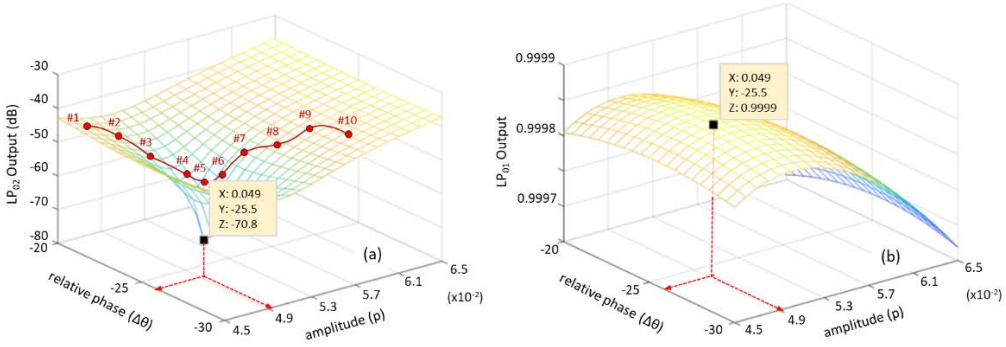

Fig. 8. (a) LP_{02} and (b) LP_{01} power at the end of the transition (diffused) region with different initially excited LP_{02} with amplitude (p) and relative phase ($\Delta\theta$) (arc duration 7s). In (a), the red superimposed line shows schematically a possible optimization path followed by progressively increasing the arc duration (Case 1) or number of short re-arcs (Case 2).

Optics EXPRESS

4. Summary and discussion

In this work, we have shown that splice optimization between dissimilar SM and MM fibres, in the presence of dopant diffusion, is a rather complex process involving coherent modal interactions. Detailed RIP measurements have shown that SMF/MMF splice area comprises three main regions characterized by 1) highly diffused and saturated EMA/EMI profile (region I), 2) fast-varying and non-adiabatic EMA/EMI changes (region II), and 3) slowly varying, quasi-adiabatic EMA/EMI changes (region III). Strong dopant diffusion over short distances in region II results in substantial RIP changes and non-adiabatic transitions over the splice length, which inevitably result in LP_{01}-to-LP_{02} power transfers, even if LP_{02} mode is not initially excited (LP_{01} only excitation – see Figs. 7 and 9(a)).

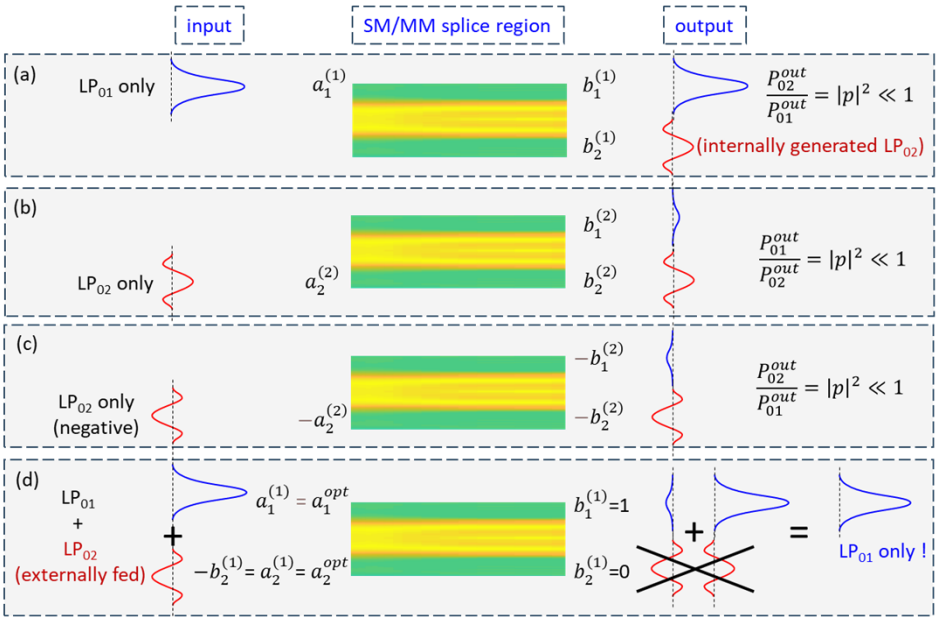

Fig. 9. SMF/MMF splice can be considered as a coaxial mode coupler: (a) LP_{01} only input results in LP_{01} & internally generated, cross-coupled LP_{02} output, with power splitting ratio $|p|^2$; (b) LP_{02} only input results in LP_{02} & LP_{01} output with same power splitting ratio |p|2; (c) reversed LP_{02} only input results in reversed LP_{02} & LP_{01} outputs; (d) due to linearity, adding inputs results in added outputs, with LP_{01} only output and LP_{02} cancelation.

In a departure from commonly used splice optimization procedures and contrary to expectations, carrying detailed RIP measurements along the splice length (using IFA) and relative LP_{02} power monitoring (using S^2 measurement set-up), we have shown that optimum splice performance, with negligible LP_{02} at the splice output, requires an EMA mismatch at the splice point ($z = 0$) and initial excitation of LP_{01} and LP_{02} mode at the splice input. This is shown schematically in Fig. 9(d). However, to nullify this power transfer and fully optimize the splice, appropriate amounts of LP_{02} and LP_{01} modes should be generated at the input of the splice with the right magnitude and phase (see Fig. 9(b) & (c)). This is achieved by an appropriate mismatch between the EMA of the LP_{01} mode on either side of the splice point ($z = 0$) (see Fig. 5(a) and Fig. 6) while the relative modal phase difference is introduced primarily over region I of the splice.

Comparing Figs. 6(a) and 7(a), it is shown that at the optimum arc duration of 7s the relative power of initially excited optimum LP_{02} mode at $z = 0$ ($|a_2^{opt}|^2 \approx 0.075$) is approximately equal to the relative power of the output LP_{02} mode ($|b_2^{(1)}|^2$), in the case of LP_{01} mode excitation

Optics EXPRESS

only, i.e. $|a_2^{opt}|^2 \approx |b_2^{(1)}|^2 \approx 0.075$. From Fig. 5(b)), on the other hand, it is shown that at the optimum arc duration of 7s, the region I length is $\Delta L_I \approx 240\,\mu m$ and the modal effective index difference is $\Delta n_{eff} \approx 2.17 \times 10^{-3}$. At an operating wavelength of $\lambda_0 = 1.07\,\mu m$, the relative phase difference of the initially excited LP_{01} and LP_{02} modes, as they enter the non-adiabatic region II, is $\Delta\varphi = (2\pi/\lambda_0)\Delta n_{eff}\Delta L_I \approx 3.06$ rad ($\approx\pi$). Therefore, these numerical data confirm the analytically obtained relation $a_2^{opt} \approx -b_2^{(1)}$ (see Eq. (6) in Appendix A). These optimization conditions, which apply to compact, non-adiabatic SMF-to-MMF splices and involve EMA mismatch and proper phasing of the initially excited LP_{01} and LP_{02} modes, are in contrast with established approaches that require near-perfect EMA matching [1,3,4] and, to the best of our knowledge, are reported for the first time. In general, this approach can be applied to splicing SMF-to-MMF or MMF-to-MMF with dissimilar core diffusion properties, regardless of their initial EMA mismatch. However, in case their initial EMAs are closely matched, the non-adiabatically HOM excitation should be avoided by reducing the arc duration (number of arcs) or increasing the length of region II and effectively turning it adiabatic.

In a manufacturing environment, where the passive and active fibers are standardized and repeatable with tight tolerances, we have shown that an optimized splicing recipe can be developed and used repeatedly in volume production.

While experimentally demonstrated in fibre splices, the significance of the work is conceptual and broadly applicable. The splice is shown to operate as a compact, reciprocal two-port modal coupler, revealing a general interference mechanism that applies to non-adiabatic fiber transitions and tapers, mode converters and beam combiners, integrated and hybrid photonic couplers, and any system where modal content is set by short, rapidly varying index perturbations.

Appendix A: two-port devices – scattering matrix description

When considering the LP_{01}/LP_{02} interactions, the SMF-to-MMF splice can be described as a general two-port device, using the scattering matrix approach. Figure 10(a) shows the splice with the two-port device (dashed rectangle) extending from just after the splice point (z = 0+) to $z = L_{spl}$, covering regions I, II and III (see Fig. 6). Modes $LP_{01}$and LP_{02} constitute port#1 and prort#2, respectively. The amplitudes of modes LP_{01} and LP_{02} at the input are a_1, a_2 while at the output are denoted as b_1 and b_2, respectively. Figure 10(b) shows the scattering matrix elements in the forward direction, while Fig. 10(c) shows the corresponding elements of the inverse scattering matrix, describing propagation through the same physical device in the backward direction.

A. Forward propagation

The scattering matrix in the forward direction is described as $S = \begin{bmatrix} s_{11} & s_{12} \\ s_{21} & s_{22} \end{bmatrix}$, where $S \in \mathbb{C}^{2x2}$, and the forward propagation is in general given by $\underline{b} = S\,\underline{a}$, where by $\underline{a} = [a_1\ a_2]^T$ and $\underline{b} = [b_1\ b_2]^T$ and $\underline{a},\ \underline{b} \in \mathbb{C}^{2x1}$. The amplitudes $b_1,\ b_2$ of the output fields are explicitly given in terms of the input fields as $b_1 = s_{11}a_1 + s_{12}a_2$ and $b_2 = s_{21}a_1 + s_{22}a_2$. The elements s_{11} and s_{21} give the portions of the input LP_{01} mode that contribute to the output LP_{01} and LP_{02} modes, respectively. Similarly, the elements s_{22} and s_{12} give the portions of the input LP_{02} mode that contribute respectively to the output LP_{02} and LP_{01} modes. In other words, s_{11} and s_{22} give the direct transmission of LP_{01} and LP_{02} modes through the splice, respectively, while s_{21} and s_{12} give the mode cross-coupling due to the non-adiabatic splice transition.

The scattering matrix elements $s_{ij}(i,j = 1,2)$ are obtained numerically by considering two special cases of launching LP_{01} and LP_{02} modes alone and using the TMM (see Supplement 1) to calculate the modal amplitudes at the splice output. For the LP_{01}-only launching, we set

Optics EXPRESS

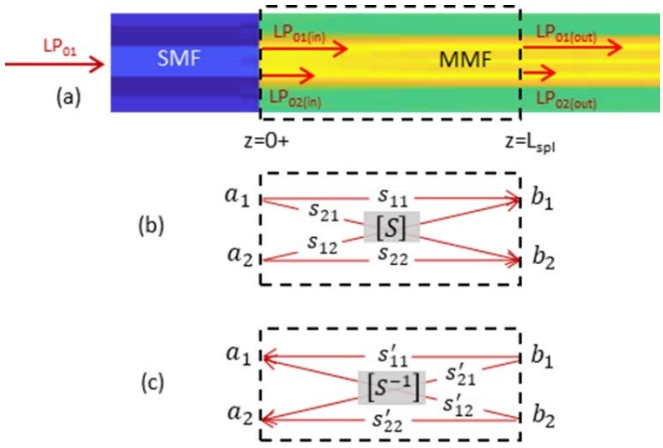

Fig. 10. (a) SMF/MMF splice as two-port device, (b) scattering matrix in forward direction, (c) inverse scattering matrix (in backward direction) elements.

$\underline{a}^{(1)} = [a_1^{(1)} \;\; a_2^{(1)}]^T = [1 \;\; 0]^T$ and obtain numerically $\underline{b}^{(1)} = [b_1^{(1)} \;\; b_2^{(1)}]^T$ while for the LP_{02}-only launching, we set $\underline{a}^{(2)} = [a_1^{(2)} \;\; a_2^{(2)}]^T = [0 \;\; 1]^T$ and obtain numerically again $\underline{b}^{(2)} = [b_1^{(2)} \;\; b_2^{(2)}]^T$. Next, by considering the scattering matrix notation, we can easily show that the corresponding scattering matrix elements are given by

$$\begin{bmatrix} s_{11} \\ s_{21} \end{bmatrix} = \begin{bmatrix} b_1^{(1)} \\ b_2^{(1)} \end{bmatrix} \quad \text{and} \quad \begin{bmatrix} s_{12} \\ s_{22} \end{bmatrix} = \begin{bmatrix} b_1^{(2)} \\ b_2^{(2)} \end{bmatrix} \tag{1}$$

B. Backward propagation

The propagation in the backward direction is described by $\underline{a} = S^{-1} \underline{b}$, where S^{-1} is the inverse of the scattering matrix S given by $S^{-1} = \frac{1}{\Delta} \begin{bmatrix} s_{22} & -s_{12} \\ -s_{21} & s_{11} \end{bmatrix}$, where $\Delta = det\{S\} = s_{11}s_{22} - s_{12}s_{21} \neq 0$ (invertible). More explicitly, in this case, the amplitudes of the waves at the input are given by:

$$\begin{aligned} a_1 &= \frac{1}{\Delta}(+s_{22}b_1 - s_{12}b_2) \\ a_2 &= \frac{1}{\Delta}(-s_{21}b_1 + s_{11}b_2) \end{aligned} \tag{2}$$

Given measured or desired outgoing waves (b_1, b_2), Eq. (1) give the incoming waves (a_1, a_2) that must have produced them or must be applied to "time-reverse" them. Indeed, if we take $\underline{a} = S^{-1} \underline{b}$ and then drive the same two-port device forward as $\underline{b}' = S \underline{a}$, we recover $\underline{b}$ exactly (assuming always that S is invertible), i.e. $\underline{b}' = S \underline{a} = S (S^{-1} \underline{b}) = (S S^{-1})\underline{b} = \underline{b}$. Mathematically, this is a perfect round-trip.

The analysis so far and Eqs. (1) and (2) apply in the general case of lossy, passive two-port devices, where $S^{\dagger}S<I$ with $S^{\dagger} = (S^{*})^T$ (Hermitian conjugate or adjoint) and I is the 2×2 identity matrix. In this case, power considerations result in $|s_{11}|^2 + |s_{21}|^2<1$ and $|s_{22}|^2 + |s_{12}|^2<1$. In all cases, for reciprocal devices, the scattering matrix S is symmetric and $s_{12} = s_{21}$. This comes from Lorentz reciprocity, which holds for linear, time invariant, passive systems without magneto-optic or other non-reciprocal effects.

Optics EXPRESS

C. Lossless two-port device

In the special case of lossless two-port devices, S is unitary and $S^{\dagger}S = SS^{\dagger} = I$. In this case, the inverse and the Hermitian conjugate are the same:

$$S^{-1} = S^{\dagger} = (S^{*})^{T} = \begin{bmatrix} s_{11}^{*} & s_{21}^{*} \\ s_{12}^{*} & s_{22}^{*} \end{bmatrix} \tag{3}$$

where (*) denotes phase conjugation. The scattering matrix elements obey the power conservation conditions $|s_{11}|^2 + |s_{21}|^2 = 1$ and $|s_{22}|^2 + |s_{12}|^2 = 1$, as well as the orthogonality relation $s_{11}^{*}s_{12} + s_{21}^{*}s_{22} = 0$. Given the reciprocity relation ($s_{12} = s_{21}$), the power conservation conditions result in $|s_{11}| = |s_{22}|$. Setting $s_{12} = s_{21} = |s_{12}|e^{-i\varphi}$ in the orthogonality relation, we obtain $s_{22} = -e^{-i2\varphi}s_{11}^{*}$ and $\Delta = det\{S\} = s_{11}s_{22} - s_{12}^{2} = -e^{-i2\varphi}$.

D. Perfect splice

A perfect splice produces only LP_{01} and no LP_{02} mode at the output, which corresponds to setting $b_1 = 1$ and $b_2 = 0$. For the general lossy case, Eq. (2) then becomes

$$\begin{aligned} a_1^{opt} &= +\frac{s_{22}}{\Delta} \\ a_2^{opt} &= -\frac{s_{21}}{\Delta} \end{aligned} \tag{4}$$

In the special case of lossless splice, using the relations derived in sub-section C above, the required input amplitudes become

$$\begin{aligned} a_1^{opt} &= s_{11}^{*} \\ a_2^{opt} &= s_{21}^{*} \end{aligned} \tag{5}$$

From Eqs. (4) and (5), it is deduced that in the case of a reciprocal, non-adiabatic splice (i.e. $s_{21} = s_{12} \neq 0$), a perfect response is achieved if both LP_{01} and LP_{02} modes are optimally excited at the input of the splice. Taking into account the definition of the scattering matrix elements $s_{ij}(i,j = 1,2)$ (see Eq. (1)), the optimum inputs for a perfect splice in the general case are given by

$$\begin{aligned} a_1^{opt} &= +\frac{1}{\Delta}b_2^{(2)} \\ a_2^{opt} &= -\frac{1}{\Delta}b_2^{(1)}, \end{aligned} \tag{6}$$

while for the lossless case they become:

$$\begin{aligned} a_1^{opt} &= b_1^{(1)*} \\ a_2^{opt} &= b_2^{(1)*} \end{aligned} \tag{7}$$

These optimum input amplitudes are required to counteract the internally generated LP_{02} mode due to the splice non-adiabaticity. We should note that non-adiabaticity occurs due to the observed significant changes in effective modal indices over rather short splice lengths, as shown in region II of Fig. 5(b). The optimum initial values a_1^{opt} and a_2^{opt} are experimentally approached by controlling the arc duration, number of arcs and/or splice post-processing. The magnitude of values a_1^{opt} and a_2^{opt} are primarily defined by the EMA mismatch at z = 0, while their phase is controlled by the length of region I (see Fig. 5(a) & (b)).

In the case of longer and adiabatic splice transition regions $s_{12} = s_{21} = 0$ and, from Eq. (4), the optimum values for the lossy case become $\begin{bmatrix} a_1^{opt} & a_2^{opt} \end{bmatrix}^T = \begin{bmatrix} s_{11}^{-1} & 0 \end{bmatrix}^T$. In this case, the

Optics EXPRESS

power conditions result in $|s_{11}|^2<1$ which means that $|a_1^{opt}|^2 = |s_{11}|^{-2}>1$. This is anticipated, since in order to achieve perfect output (i.e. $|b_1|^2 = 1;\ |b_2|^2 = 0$) in an adiabatic ($s_{12} = s_{21} = 0$) lossy splice, the normalised input power of the LP_{01} mode should be larger than 1 (i.e. $|a_1|^2>1$). However, for the lossless, adiabatic case the optimum input fields for a perfect splice become $\begin{bmatrix} a_1^{opt} & a_2^{opt} \end{bmatrix}^T = \begin{bmatrix} 1 & 0 \end{bmatrix}^T$. In this case, EMA matching between LP_{01} modes on either side of the splice ($z = 0$) is required only, which is the standard traditional splice optimization process [3–6].

Funding. Engineering and Physical Sciences Research Council (EP/P027644/1, EP/W028786/1).

Acknowledgment. The authors acknowledge useful discussions with Dr. Fabio Ghiringelli and Dr. Mike Durkin.

Disclosures. The authors declare no conflicts of interest.

Data availability. Data underlying the results presented in this paper are not publicly available at this time but may be obtained from the authors upon reasonable request.

Supplemental document. See Supplement 1 for supporting content.

References

1. A. D. Yablon, *Optical Fiber Fusion Splicing* (Springer, 2005).
2. D. Marcuse, "Loss analysis of single-mode fiber splices," Bell Syst. Tech. J. **56**(5), 703–718 (1977).
3. B. S. Wang and E. W. Mies, "Optical Coupling Optimization for Fiber Lasers and Devices," Proc. SPIE **7134**, 71341I–71341I-6 (2008).
4. A. D. Yablon, M.F. Yan, D.J. DiGiovanni, *et al.*, "Frozen-In Viscoelasticity for Novel Beam Expanders and High-Power Connectors," J. Lightwave Technol. **22**(1), 16–23 (2004).
5. H. Y. Tam, "Simple splicing for reducing loss between single-mode fibers and erbium-doped fiber," Electron. Lett. **27**(17), 1597–1599 (1991).
6. W. Zheng, O. Hulten, and R. Rylander, "Erbium-doped fiber splicing and splice loss estimation," J. Lightwave Technol. **12**(3), 430–435 (1994).
7. L. Zhang, L. Pei, J. Wang, *et al.*, "Observation of mode evolution between active and passive fibres with intrinsic microstructure characterisation," IEEE Trans. Instrum. Meas. **74**, 1–9 (2025).
8. J. T. Krause, W. A. Reed, and K. L. Walker, "Splice loss of single-mode fiber as related to fusion time, temperature and index profile alteration," J. Lightwave Technol. **4**(7), 837–840 (1986).
9. J. Luo, "Modeling dissimilar optical fiber splices with substantial diffusion," J. Lightwave Technol. **25**(11), 3575–3579 (2007).
10. H. Renner, "Bending losses of coated single-mode fibers: a simple approach," J. Lightwave Technol. **10**(5), 544–551 (1992).
11. M. N. Zervas and C. A. Codemard, "High power fiber lasers: a review," J. Select. Top. Quantum Electron. **20**(5), 219–241 (2014).
12. T. Eidam, C. Wirth, C. Jauregui, *et al.*, "Experimental observations of the threshold-like onset of mode instabilities in high power fiber amplifiers," Opt Express **19**(14), 13218–13224 (2011).
13. V. Scarnera, F. Ghiringelli, A. Malinowski, *et al.*, "Modal instabilities in high power fiber laser oscillators," Opt. Express **27**(4), 4386–4403 (2019).
14. J. W. Nicholson, A. D. Yablon, S. Ramachandran, *et al.*, "Spatially and spectrally resolved imaging of modal content in large-mode-area fibers," Opt. Express **16**(10), 7233–7243 (2008).
15. M. Tachikura, "Fusion mass-splicing for optical fibers using electric discharges between two pairs of electrodes," Appl. Opt. **23**(3), 492–498 (1984).
16. K. Morishita, "Numerical analysis of pulse broadening in graded index optical fibers," IEEE Microwave Theor. Techn. **29**(4), 348–352 (1981).
17. W. Burns and F. Milton, "Mode conversion in planar-dielectric separating waveguides," IEEE J. Quantum Electron. **11**(1), 32–39 (1975).
18. J. W. Fleming and C. R. Kurkjian, "Measurement of cation diffusion in silica light guides," J. Am. Ceram. Soc. **68**(9), C-246–C-248 (1985).
19. J. Kirchhof, S. Unger, B. Knappe, *et al.*, "Diffusion of binary GeO_2-SiO_2 glasses," Phys. Chem. Glasses: Eur. J. Glass Sci. Technol. B **48**(3), 129–133 (2007).
20. A. C. Boucouvalas, "Coaxial optical fiber coupling," J. Lightwave Technol. **3**(5), 1151–1158 (1985).
21. A.C. Boucouvalas and G. Georgiou, "Concatenated, tapered coaxial coupler filters," IEE Proc. **134**(3), 191–195 (1987).